THE JOURNAL OF BIOLOGICAL CHEMISTRY VOL. 281, NO. 40, pp. 29817–29829, October 6, 2006

Structural and Functional Characterization of Transmembrane Segment VII of the Na^+/H^+ Exchanger Isoform 1*[S]

Received for publication, June 27, 2006, and in revised form, July 20, 2006 Published, JBC Papers in Press, July 21, 2006, DOI 10.1074/jbc.M606152200

Jie Ding[‡1,2], **Jan K. Rainey**[‡§1,3], **Caroline Xu**[‡], **Brian D. Sykes**[‡§4], **and Larry Fliegel**[‡5]

From the [‡]*Department of Biochemistry and* [§]*Protein Engineering Network of Centres of Excellence, University of Alberta, Edmonton, Alberta T6G 2H7, Canada*

The Na^+/H^+ exchanger isoform 1 is an integral membrane protein that regulates intracellular pH by exchanging one intracellular H^+ for one extracellular Na^+. It is composed of an N-terminal membrane domain of 12 transmembrane segments and an intracellular C-terminal regulatory domain. We characterized the structural and functional aspects of the critical transmembrane segment VII (TM VII, residues 251–273) by using alanine scanning mutagenesis and high resolution NMR. Each residue of TM VII was mutated to alanine, the full-length protein expressed, and its activity characterized. TM VII was sensitive to mutation. Mutations at 13 of 22 residues resulted in severely reduced activity, whereas other mutants exhibited varying degrees of decreases in activity. The impaired activities sometimes resulted from low expression and/or low surface targeting. Three of the alanine scanning mutant proteins displayed increased, and two displayed decreased resistance to the Na^+/H^+ exchanger isoform 1 inhibitor EMD87580. The structure of a peptide of TM VII was determined by using high resolution NMR in dodecylphosphocholine micelles. TM VII is predominantly α-helical, with a break in the helix at the functionally critical residues Gly^{261}–Glu^{262}. The relative positions and orientations of the N- and C-terminal helical segments are seen to vary about this extended segment in the ensemble of NMR structures. Our results show that TM VII is a critical transmembrane segment structured as an interrupted helix, with several residues that are essential to both protein function and sensitivity to inhibition.

The mammalian Na^+/H^+ exchanger isoform 1 (NHE1)[6] is a ubiquitous integral membrane protein mediating removal of a single intracellular proton in exchange for one extracellular sodium ion (1). NHE1 has several cellular and physiological functions, including protecting cells from intracellular acidification (2, 3), promoting cell growth and differentiation (2), and regulating sodium fluxes and cell volume after osmotic shrinkage (4). The Na^+/H^+ exchanger also plays a critical role in the damage that occurs during ischemia and reperfusion and may play a key role in mediating heart hypertrophy. Inhibition of the exchanger protects the myocardium in these two forms of heart disease (5, 6). Amiloride and its derivatives are inhibitors of the NHE1 isoform of the Na^+/H^+ exchanger, and a new generation of Na^+/H^+ exchanger inhibitors is being developed for clinical treatment of heart disease (7, 8). In addition to these many physiological roles, more recently, the Na^+/H^+ exchanger has been demonstrated to be involved in modulating cell motility and invasiveness of neoplastic breast cancer cells (9) and has been shown to be critical to cell motility in some cell types (10).

NHE1 is composed of two domains as follows: an N-terminal membrane domain of ~500 amino acids and a C-terminal regulatory domain of ~315 amino acids (1, 6). The N-terminal membrane domain is responsible for ion movement and has 12 transmembrane segments and 3 membrane-associated segments (11) (Fig. 1*A*). How this domain binds and transports Na^+ ions and protons is only recently starting to be elucidated. We have recently analyzed TM IV of the NHE1 isoform of the Na^+/H^+ exchanger. We showed that prolines 167 and 168 are critical to NHE1 function, targeting, and expression (12). Phe^{161} was shown to be a pore-lining residue critical to transport, and the structure of TM IV was shown to be atypical of TM proteins, being composed of one region of β-turns, an extended middle region, including Pro^{167}–Pro^{168}, plus a region helical in character (13).

* The costs of publication of this article were defrayed in part by the payment of page charges. This article must therefore be hereby marked "*advertisement*" in accordance with 18 U.S.C. Section 1734 solely to indicate this fact.

The atomic coordinates and structure factors (code 2HTG) have been deposited in the Protein Data Bank, Research Collaboratory for Structural Bioinformatics, Rutgers University, New Brunswick, NJ (http://www.rcsb.org/).

[S] The on-line version of this article (available at http://www.jbc.org) contains supplemental text, Figs. S1 and S2, and supplemental Refs. 1–10.

[1] Both authors contributed equally to this work.

[2] Supported by Alberta Heritage Foundation for Medical Research and the Canadian Institutes of Health Research Strategic Training Institute in Membrane Proteins and Cardiovascular Disease.

[3] Recipient of postdoctoral fellowships from the Natural Sciences and Engineering Research Council of Canada, the Alberta Heritage Foundation for Medical Research, and the Canadian Institutes of Health Research Strategic Training Institute in Membrane Proteins and Cardiovascular Disease.

[4] Recipient of support as a Canada Research Chair in Structural Biology.

[5] Supported by a grant from the Canadian Institutes of Health Research and a Scientist Award from Alberta Heritage Foundation for Medical Research. To whom correspondence should be addressed: Dept. of Biochemistry, 347 Medical Science Bldg., University of Alberta, Edmonton, Alberta T6G 2H7, Canada. Tel.: 780-492-1848; Fax: 780-492-0886; E-mail: lfliegel@ualberta.ca.

[6] The abbreviations used are: NHE1, Na^+/H^+ exchanger isoform 1; DIPSI, decoupling in the presence of scalar interactions; DPC, dodecylphosphocholine; DPC-d_{38}, deuterated DPC; HA, hemagglutinin; HSQC, heteronuclear single quantum coherence spectroscopy; NOE, nuclear Overhauser effect; NOESY, NOE spectroscopy; PBS, phosphate-buffered saline; TM, transmembrane (segment); TOCSY, total correlation spectroscopy; HPLC, high pressure liquid chromatography; *t*-Boc, *tert*-butyloxycarbonyl.

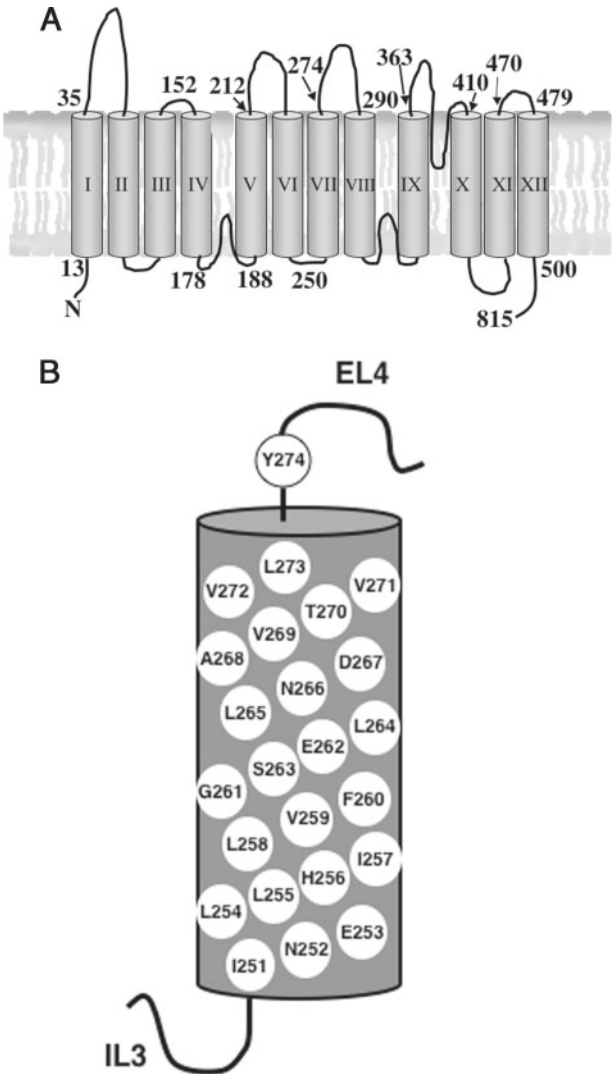

FIGURE 1. **Models of the Na^+/H^+ exchanger.** *A,* topological model of the transmembrane domain of the NHE1 isoform of the Na^+/H^+ exchanger as described earlier (11). *B,* model of amino acids present in TM VII.

TM VII is believed to extend from amino acids Ile^{251} to Leu^{273} (11) (Fig. 1*B*). We have shown that TM VII is critical for the function of the NHE1 isoform of the Na^+/H^+ exchanger (14). We demonstrated that Glu^{262} and Asp^{267} of TM VII are critical for activity. Residues with a similar position and charge in TM VI were not important. The E262Q and D267N mutations destroyed activity of the NHE, whereas replacement with the other negatively charged amino acid retained, but modified, exchanger activity. In this study, we examine both structural and functional aspects of TM VII of the NHE1 isoform of the Na^+/H^+ exchanger. We use alanine scanning and insertional mutagenesis (15, 16) to determine amino acid residues critical for Na^+/H^+ exchanger activity, expression, targeting, and inhibitor resistance. We also use NMR to examine the structure of an isolated transmembrane segment. It must be acknowledged that an isolated membrane segment could have a different structure than that found in an intact membrane protein. However, isolated TM segments from membrane proteins having multiple TM segments, including the cystic fibrosis transmembrane conductance regulator (17, 18), bacteriorhodopsin (19, 20), rhodopsin (21), and the fungal G-protein-coupled receptor Ste2p (22), have been shown to be both functional and to have structures in good agreement with the segments in the context of the entire protein, where available. An important caveat is that solution conditions may need extensive screening in order to achieve stabilization of the peptide in its physiological structure, for example, the variation in bacteriorhodopsin results of Ref. 19 *versus* Ref. 20 and our previous study of TM IV of NHE1 (13). Following from this body of work, the TM VII peptide was chemically synthesized and used to determine its structure in dodecylphosphocholine (DPC) micelles. The use of DPC micelles as a membrane mimetic environment in the solution state has been well established through structural studies of both membrane-spanning and membrane-associated proteins or peptides (23, 24). Our study demonstrates that TM VII is structured as an interrupted, likely kinked α-helix. We identify residues critical in transport and those that modify inhibitor resistance. TM VII is distinctly different from TM IV in both its structure and in functional aspects.

EXPERIMENTAL PROCEDURES

Materials—EMD87580 was a generous gift of Dr. N. Beier of Merck. PWO DNA polymerase was from Roche Applied Science, and Lipofectamine™ 2000 reagent was from Invitrogen. ^{15}N-Labeled, *t*-Boc-protected amino acids and deuterated solvents were purchased from Cambridge Isotope Laboratories (Andover, MA). Deuterated SDS and DPC were purchased from C/D/N Isotopes (Pointe-Claire, Quebec, Canada) and used without further purification.

Site-directed Mutagenesis—To examine and characterize critical amino acids of TM VII of the Na^+/H^+ exchanger, mutations were made to an expression plasmid containing a hemagglutinin (HA)-tagged human NHE1 isoform of the Na^+/H^+ exchanger. The plasmid pYN4+ contains the cDNA of the entire coding region of the Na^+/H^+ exchanger (12). Two series of mutants were made (Table 1). One series of mutants was made in which all the residues of TM VII were mutated to alanine. A second series was for insertional mutagenesis, whereby alanine residues were inserted at critical locations between residues of TM VII in the wild type pYN4+. Two alanine insertional mutants were made, one inserting an alanine between Gly^{261} and Glu^{262}, and a second inserting an alanine between Leu^{264} and Leu^{265}. A third insertional mutant had two mutations, a glutamate inserted between Gly^{261} and Glu^{262} plus an N266D mutation. Site-directed mutagenesis using amplification with PWO DNA polymerase (Roche Applied Science) was followed by using the Stratagene (La Jolla, CA) QuikChange™ site-directed mutagenesis kit. Mutations created a new restriction enzyme site for use in screening transformants. DNA sequencing confirmed the mutations and fidelity of PCR.

Cell Culture and Transfections—To examine Na^+/H^+ exchanger expression and activity, AP-1 cells were used that lack an endogenous Na^+/H^+ exchanger (14). Transfection with Lipofectamine™ 2000 reagent (Invitrogen) was used to make stable cell lines of all mutants as described earlier (12). Transfected cells were selected using 800 μg/ml geneticin (G418),

TABLE 1

Oligonucleotides used for site-directed mutagenesis

Mutated nucleotides are in lowercase letters and boldface type. Mutated amino acid residues are indicated using single letter notation, and new restriction sites are underlined. Restriction sites deleted are indicated in parentheses. Amino acids flanking the insert are indicated where insertional mutagenesis occurred. Top, oligonucleotides used for alanine scanning mutagenesis. Bottom, synthetic oligonucleotides used for alanine insertional mutagenesis.

Mutation	Oligonucleotide sequence (alanine scanning)	Restriction site
I251A	5′-GAGGAAATTCACgcgAATGAGCTGCTG-3′	BcgI
N252A	5′-GGAAATTCACATCgcTGAGCTcCTGCACATCCTTG-3′	SstI
E253A	5′-TTCACATCAATGcGCTcCTcCACATCCTTGTTTTTG-3′	BseRI1
L254A	5′-CACATCAATGAagcttTGCACATCCTTG-3′	HindIII
L255A	5′-CATCAATGAGCTagcGCACATCCTTG-3′	NheI
H256A	5′-CAATGAGCTGCTagcCATCCTTGTTTTTGG-3′	NheI
I257A	5′-CAATGAGCTGCTGCAtgcCCTTGTTTTTGGG-3′	SphI
L258A	5′-GAGCTGCTGCAtATCgcTGTTTTTGGGGAG-3′	(BsgI)
V259A	5′-GCTGCACATCCTTgcaTTcGGGGAGTCCTTGC-3′	BsmI
F260A	5′-GCACATCCTTGTTgccGGcGAGTCCTTGCTC-3′	NaeI
G261A	5′-CATCCTTGTTTTTGcGGAaagCTTGCTCAATGACG-3′	HindIII
E262A	5′-CCTTGTTTTTGGGGcaagCTTGCTCAATGACG-3′	HindIII
S263A	5′-CTTGTTTTTGGGGAGgCCTTGCTCAATGAC-3′	StuI
L264A	5′-GTTTTTGGGGAGTCCgcttTaAATGACGCCGTCAC-3′	DraI
L265A	5′-GTTTTTGGGGAGTCCcTcgcgAATGACGCCGTCAC-3′	NruI
N266A	5′-TTGGGAGTCCTTGCTagcTGACGCCGTCACTG-3′	NheI
D267A	5′-GTCCTTGCTCAATGctGCaGTCACTGTGGTCC-3′	PstI
V269A	5′-CTCAATGACGCCGcgACTGTGGTgCTGTATC-3′	BcgI
T270A	5′-CAATGACGCCGTCgCgGTcGTCCTGTATCAC-3′	BsiEI
V271A	5′-GACGCCGTCACTGcaGTCCTGTATCACC-3′	PstI
V272A	5′-GACGCCGTCACgGTcgcCCTGTATCACCTC-3′	BsiEI
L273A	5′-GTCACTGTGGTCgcGTATCACCTCTTTG-3′	(AvaII)

Mutation	Oligonucleotide sequence	Restriction site
G261-A-262E	5′-CACATCCTTGTTTTTGG**cgcc**GAGTCCTTGCTCAATGACG-3′	NarI
L264-A-265L	5′-GGGAGTCCTT**agcgCTCAATGACG**-3′	Eco47III
G261-E-262E	5′-TGTTTTTGGG**gagGAaag**cttgcTCAATG-3′	HindIII
N266D	GTCCTTGCTCgAcgacgccGTCAC	DrdI

and stable cell lines for experiments were regularly re-established from frozen stocks at passage numbers between 5 and 9.

SDS-PAGE and Immunoblotting—To confirm NHE1 expression, cell lysates were made from AP-1 cells as described earlier (12). For Western blot analysis, equal amounts of up to 100 μg of each sample were resolved on 10% SDS-polyacrylamide gels. Nitrocellulose transfers were immunostained using anti-HA monoclonal antibody (Roche Applied Science) and peroxidase-conjugated goat anti-mouse antibody (Bio/Can, Mississauga, Ontario, Canada). The enhanced chemiluminescence Western blotting and detection system (Amersham Biosciences) was used to visualize immunoreactive proteins. Densitometric analysis of x-ray films was using NIH Image 1.63 software (National Institutes of Health, Bethesda).

Cell Surface Expression—Cell surface expression was measured with sulfo-NHS-SS-biotin (Pierce) essentially as described earlier (12). Briefly, the cell surface was labeled with sulfo-NHS-SS-biotin, and immobilized streptavidin resin was used to remove plasma membrane Na^+/H^+ exchanger. Equivalent amounts of the total and unbound proteins were analyzed by SDS-PAGE followed by Western blotting and densitometry as described above. The relative amount of NHE1 on the cell surface was calculated by comparing both the 110- and the 95-kDa HA-immunoreactive species in Western blots of the total and unbound fractions.

Na^+/H^+ Exchange Activity—Na^+/H^+ exchange activity was measured using a PTI Deltascan spectrofluorometer. The initial rate of Na^+-induced recovery of cytosolic pH (pH_i) was measured after ammonium chloride-induced acute acid load using 2′,7′-bis(carboxyethyl)-5,6-carboxyfluorescein-AM (Molecular Probes Inc., Eugene, OR). Recovery was in the presence of 135 mM NaCl and was measured as described previously (13). There was no difference in the buffering capacities of stable cell lines as indicated by the degree of acidification induced by ammonium chloride. For some experiments cells were treated with EMD87580 of varying concentrations. EMD87580 was dissolved in water, and the inhibitory effect of EMD87580 was documented using a two-pulse acidification assay. Cells were treated with ammonium chloride two times and allowed to recover in NaCl-containing medium. One pulse was in the absence of EMD87580 and one in the presence of inhibitor. The rate of recovery from acid load was compared ± inhibitor. Where indicated, the activity of the Na^+/H^+ exchanger mutants was corrected for the level of protein expression and for the targeting of the protein to the cell surface. Results are shown as mean ± S.E., and statistical significance was determined using the Mann-Whitney *U* test.

Peptide Synthesis and Purification—TM VII peptides (sequence, HINELLHILVFGESLLNDAVTVVLYKK; free N terminus, amide-capped C terminus) with and without selective ^{15}N labels were synthesized and purified using previously published *t*-Boc solid-phase techniques optimized for hydrophobic membrane-spanning peptides (25), with the difference that purification was carried out using a Zorbax 300 SB-C3 9.4-mm × 25-cm HPLC column (Agilent Technologies, Palo Alto, CA). Peptide identity was confirmed by matrix-assisted laser desorption ionization mass spectrometry and by amino acid analysis.

NMR Spectroscopy and Structure Calculation—Samples for structural study were obtained by dissolving ~1 mM synthetic TM VII peptide in 90% H_2O, 10% D_2O solution containing ~75 mM DPC-d_{38}. Chemical shifts were referenced to 2,2-dimeth-

yl-2-silapentane-5-sulfonic acid at 1.0 mM, with indirect referencing employed for ^{15}N (26). Solution pH was adjusted to 4.8 (deuterium isotope effects not taken into account), and all experiments were carried out at 30 °C. One-dimensional ^{1}H, natural abundance gradient-enhanced ^{1}H-^{13}C HSQC, TOCSY (60-ms mix; DIPSI spin lock), and NOESY (225–250-ms mix) experiments were acquired on the Canadian National High Field NMR Centre Varian INOVA 800-MHz spectrometer for each sample. With the selectively ^{15}N-labeled peptide, additional three-dimensional ^{15}N-edited NOESY-HSQC (250-ms mix) and TOCSY-HSQC (57-ms mix, DIPSI spin lock) experiments were acquired at 500-MHz on a Varian Inova spectrometer. All experiments were used as configured within the Varian BioPack software package. Spectra were processed using NMRPipe (27) and analyzed using Sparky 3 (T. D. Goddard and D. G. Kneller, University of California, San Francisco).

Structure calculation was carried out in the python scripting interface of XPLOR-NIH version 2.13 (28) using NOE restraints derived from the 225- and 250-ms mixing time experiments at 800 MHz. Homonuclear NOESY peaks were manually picked in Sparky, and volumes were calculated using Gaussian fits, with motion of the peak center generally allowed; in some cases (~1.5%) in the NOESY spectra, Sparky's gaussian fit algorithm did not find a convergent solution, and a summed signal intensity was used instead over a manually specified region. Initial NOE calibration was carried out empirically from peak volumes to provide a value in the range of 1.8–6.0 Å; this was carried out separately for each spectrum in order to normalize for mixing time. These estimates were used to bin each restraint into one of strong (1.8–2.8 Å), medium (1.8–3.6 Å), weak (1.8–5.0 Å), or very weak (1.8–6.0 Å). Ambiguous assignments were handled using the XPLOR-NIH "or" statement, with the "sum" averaging option employed and the "number of monomers" parameter set to 1. The NOE term used the hard (square well) potential with a scaling factor of 20 for the high temperature stage and a ramped scaling factor over the range 1–30 for the cooling stage. The dihedral angle potential used a constant scaling factor of 5 (rounds 1–8) or 25 (rounds 9–10) throughout the annealing protocol. Families of structures were generated using simulated annealing with a high temperature stage at 3500 K of length 20 ps and a slow cooling stage going from 3500 to 100 K in 25 K temperature steps for 2-ps stages. Time steps of 10 fs were used in each case.

Structure calculations were carried out in two different manners. In one, a single extended polypeptide was generated and subjected to simulated annealing. In the other, two extended polypeptides with identical TM VII primary sequence were generated. In this case, each intra-residue NOE was doubled to apply to each conformer. All other NOEs were made ambiguous, allowing satisfaction through the XPLOR-NIH summed average by any combination of intra-polypeptide and inter-polypeptide NOE restraints. To handle the multiple conformations of the TM VII peptide being produced and to allow practical generation and analysis of numerous ambiguous restraints, an in-house tcl/tk script (freely available upon request) was used to iteratively refine the NOE restraints. As will be discussed below, use of two conformations allowed satisfaction of all NOE restraints, whereas a single conformation required significant pruning of the family of NOE restraints. Analysis and NOE refinement are therefore only described for the two-conformer calculation. Families of 50–200 structures were generated, and NOE violations were analyzed over each ensemble of structures. A series of NOE restraint refinements was carried out. Initially, violations >0.5 Å in >50% of structures were lengthened by one category; over subsequent rounds, the violation threshold was subsequently decreased incrementally to 0.05 Å and the number of violators to >10%. After 8 cycles of simulated annealing and NOE refinement, calculated XPLOR-NIH structure energies contained minimal contributions from NOE violations; violations were not observed in >10% of the ensemble for any NOEs, and magnitudes of all observed violations were minimal. Two further cycles of simulated annealing were carried out with increased weighting on the dihedral angle restraints with further, very minor, NOE restraint refinements carried out using the most stringent bounds given above between rounds 9 and 10. From this ensemble of 60 two-conformer structures, the lowest energy 33 ensemble members (selected based upon an arbitrary cutoff of 60 kcal/mol in XPLOR-NIH total energy values) containing 66 polypeptide conformers were retained for further analysis. The final sets of restraints have been deposited in the Protein Data Bank (entry 2HTG) along with this ensemble of structures.

RESULTS

Alanine Scanning Mutagenesis—To determine which amino acids of TM VII were critical to targeting, expression, and activity, we mutated each amino acid of this transmembrane segment to alanine. Fig. 2, *A–C,* illustrates a Western blot demonstrating expression of the NHE alanine scanning mutants in AP-1 cells stably transfected with HA-tagged Na^+/H^+ exchanger. The expression levels of the Na^+/H^+ exchanger varied slightly from one stable cell line to another. All of the mutants expressed the protein although the levels varied from 31 to 149% of the control. All mutants expressed the 110-kDa glycosylated form of the protein and a smaller 95-kDa unglycosylated form of the protein. We have earlier shown that unglycosylated Na^+/H^+ exchanger may be functional (29); therefore, the unglycosylated protein was included in analysis of the levels of protein expression. The E262A mutant was found predominantly as unglycosylated protein, similar to the E262Q mutation that we reporter earlier (14). All other mutants were found as predominantly 110-kDa isoforms. Expression of L254A, E262A, V272A, and L273A was less than 60% of the control value.

We have shown earlier (13) that mutation of amino acids of transmembrane segments can affect surface targeting of the Na^+/H^+ exchanger. Therefore, we examined intracellular targeting of the NHE1 expressing cell lines within AP-1 cells. Cells were treated with sulfo-NHS-SS-biotin and then lysed and solubilized, and labeled proteins were bound to streptavidin-agarose beads. Equal amounts of total cell lysates and unbound lysates were separated by size using SDS-PAGE, and Western blotting with anti-HA antibody identified the tagged NHE1 protein. Fig. 3 (*first 24 panels*) illustrates examples of the results and a summary of quantification of at least six experiments.

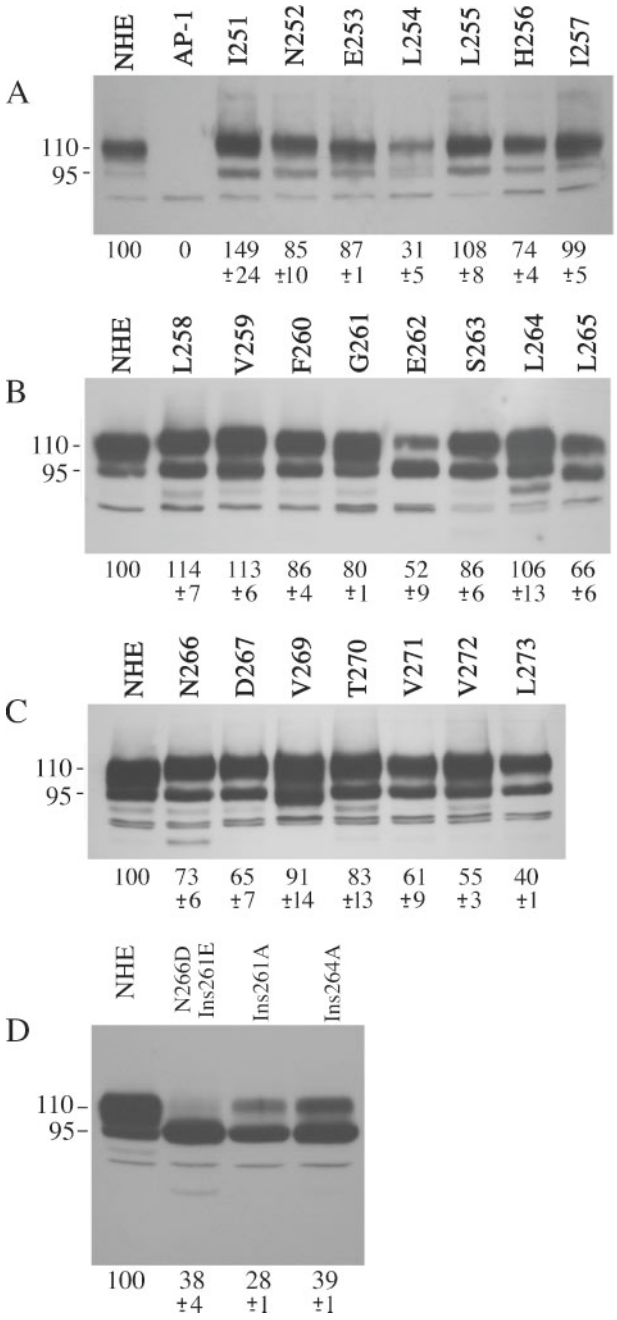

FIGURE 2. **Western blot analysis of cell extracts from control and stably transfected AP-1 cells with mutations in TM VII.** Cell extracts were prepared from control and stably transfected cell lines. In all mutations the amino acid indicated was changed to alanine. 100 μg of total protein was loaded in each lane. *Numbers below* the lanes indicate the values obtained from densitometric scans of both the 110- and 95-kDa bands relative to wild type NHE. Results are mean ± the S.E. of at least three measurements. *A–C* are extracts from stable cells lines of alanine scanning mutants of amino acids Ile^{251}–Leu^{273}. NHE refers to samples of cells extracts containing the wild type Na^+/H^+ exchanger. AP-1 refers to extracts from AP-1 cells not-transfected with Na^+/H^+ exchanger. *D* contains control (NHE) cell extracts plus extracts from cells containing alanine insertional mutants. N266DIns261E contains the mutant NHE with Asn^{266} changed to Asp and an glutamic acid inserted after amino acid 261. Ins261A and Ins264A are extracts from cells with NHE containing alanine inserted after amino acids 261 and 264, respectively.

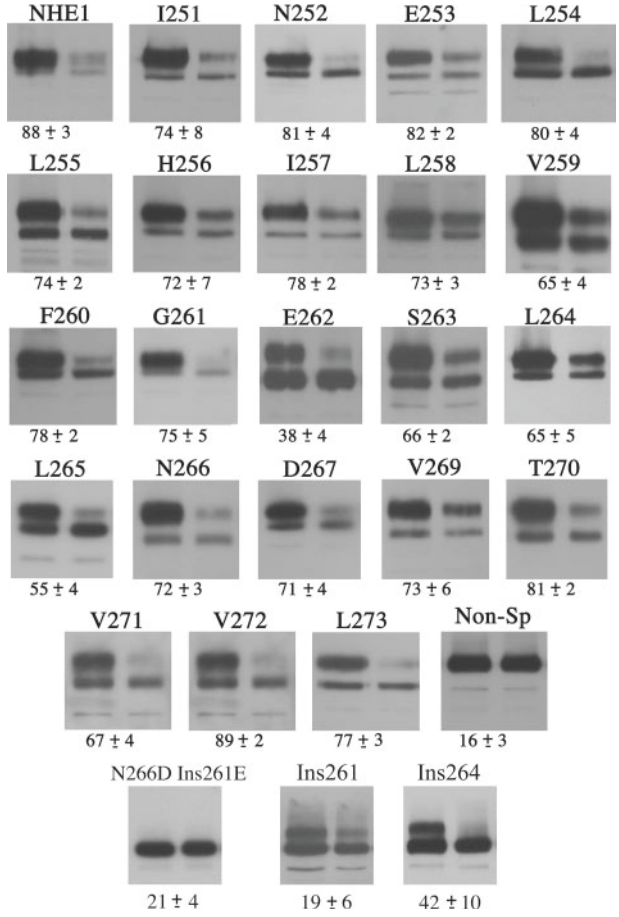

FIGURE 3. **Subcellular localization of control NHE and TM VII mutants in AP-1 cells.** Sulfo-NHS-SS-biotin-treated cells were lysed, and solubilized proteins were treated with streptavidin-agarose beads to bind labeled proteins as described under "Experimental Procedures." Equal samples of total cell lysate (*left side* of panel) and unbound lysate (*right side* of panel) were run on SDS-PAGE. Western blotting with anti-HA antibody identified NHE1 protein. In all mutations the amino acid indicated was changed to alanine. *Non-Sp* refers to an experiment in which nonspecific binding to streptavidin-agarose beads was carried out following the standard procedure but without labeling cells with biotin. The *bottom row* is from cells containing alanine insertional mutations as described in Fig. 2. The percent of the total NHE1 protein that was found within the plasma membrane is indicated for each mutant. For nonspecific binding the numbers indicate the amount of nonspecific binding to streptavidin-agarose beads. The results are the mean ± the S.E. of at least six determinations.

Both the 110- and 95-kDa bands were included in the analysis. The Glu^{262} mutant was found principally in intracellular compartments. Mostly this was as the 95-kDa unglycosylated form of the protein. Nonspecific binding of NHE1 protein to streptavidin-agarose beads was ~16%, so the values shown overestimate the level of surface protein.

We determined how the mutations of the protein affected the activity. The rate of recovery from an acute acid load was determined as described earlier (30). Fig. 4*A* illustrates the rates of recovery from stable cell lines transfected with either wild type Na^+/H^+ exchanger or mutants of TM VII. The rate of recovery is also shown when corrected for both the level of expression and surface targeting. The mutants fell into several general categories. Some had less than 50% of wild type activity, when measuring the activity uncorrected for expression levels and targeting. This included Leu^{254}, Leu^{255}, His^{256}, Ile^{257}, Val^{259}, Phe^{260}, Gly^{261}, Glu^{262}, Asn^{266}, Asp^{267}, Thr^{270}, Val^{271}, and Val^{272}. Within this group of mutants with reduced activity, there were subgroups of mutants. One subgroup had direct effects on Na^+/H^+ exchanger activity. Even after correcting for

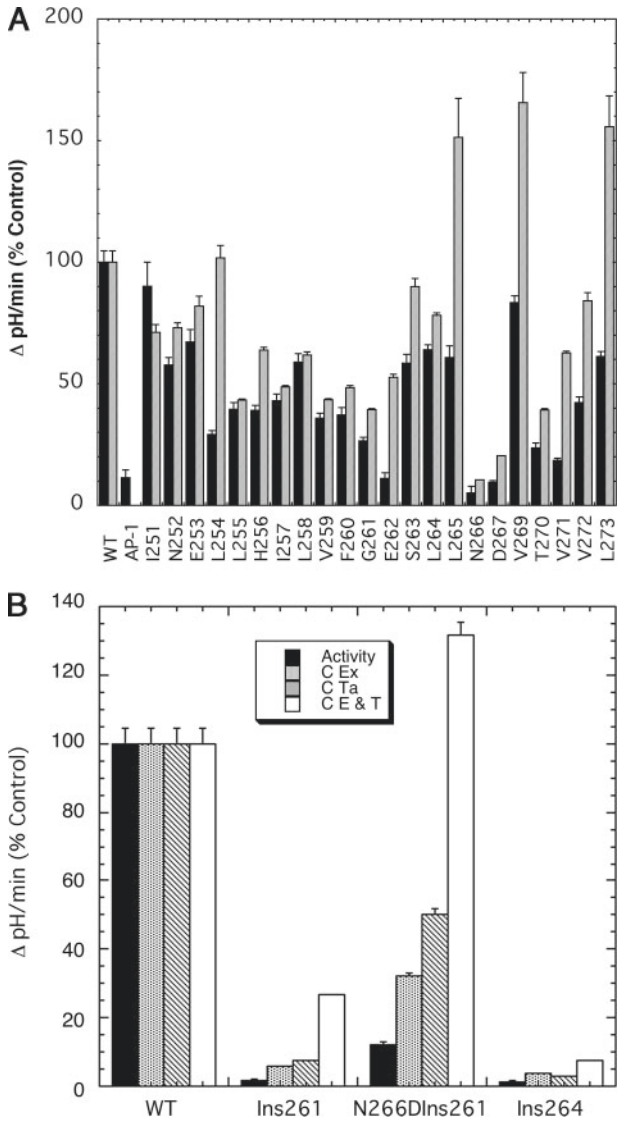

FIGURE 4. **Na^+/H^+ exchanger activity of cell lines expressing control and NHE1 mutants.** NHE activity was measured as described under "Experimental Procedures" in stable cell lines expressing NHE1. *WT*, wild type NHE1. *A*, alanine scanning mutants with the mutation indicated. *Hatched bars* indicate the activity after correction for the level of expression and surface targeting. *Solid bars* are uncorrected. *B*, alanine insertional mutations as described in Fig. 2. The activity of each mutant was measured and was then corrected relative to controls for the level of expression of protein, for targeting to the cell surface, and for both the level of expression (*Ex*) and targeting (*Ta*). The results are the mean ± the S.E. of at least six determinations from two independently made cell lines.

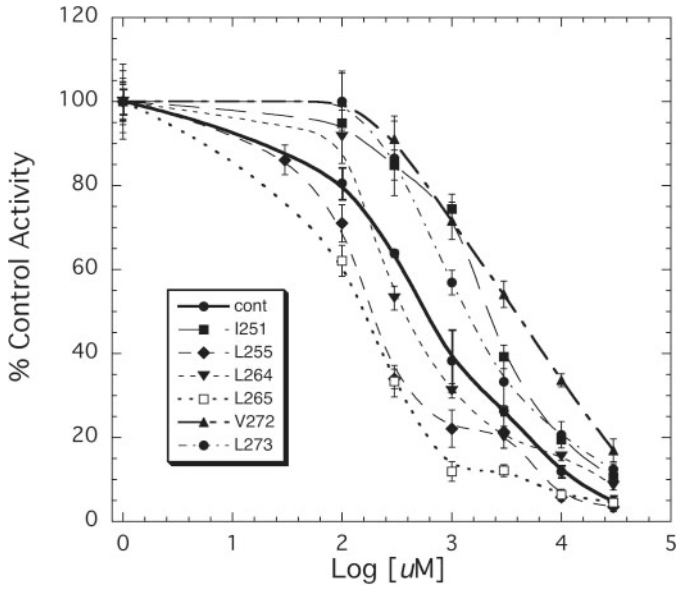

FIGURE 5. **Dose-response curves for inhibition by EMD87580 of the initial rates of recovery from an NH4Cl prepulse in stable cell lines expressing control and NHE1 mutants.** Results are presented as the percentage of efflux from control cells without inhibitor. Increasing concentrations were used. Results are the mean ± the S.E. of at least six determinations. *Cont*, control.

targeting and the level of expression, the activity was 50% or more reduced compared with controls. This subgroup included Leu^{255}, Ile^{257}, Val^{259}, Phe^{260}, Gly^{261}, Asn^{266}, Asp^{267}, and Thr^{270}. Mutant N266A was not active in contrast to our previous report (14). We determined that the earlier results were because of a spontaneous reversion of the mutation (not shown). A different subgroup had reduced expression or targeting to the cell surface, and when correcting for these factors, activity of the mutants was increased to over 60% of controls. This subgroup included Leu^{254}, His^{256}, Glu^{262}, Val^{271}, and Val^{272}. These mutants therefore had normal or relatively normal Na^+/H^+ exchanger activity but mutations that affected their targeting or expression. For all of this subgroup except Glu^{262}, most of the abnormality in observed, uncorrected activity was because of effects on expression of the protein (Fig. 2). For the Glu^{262} mutant, the reduced activity was because of effects on both targeting and expression levels. Glu^{262} was the only alanine scanning mutation that caused major effects on targeting. However, even after correcting for targeting and expression, the corrected activity of Glu^{262} was only 52% of the control levels indicating there was still a significant defect in the Na^+/H^+ exchanger activity. There was a different group of mutants (Leu^{265}, Val^{269}, and Leu^{273}) that had greater than 50% of control Na^+/H^+ exchanger activity prior to correction for effects on targeting. After correction for targeting and protein expression, they had activity that was greater than that of controls.

Amiloride analogs have been used as specific inhibitors of the Na^+/H^+ exchanger. A variety of studies have shown that mutations in specific amino acids of the transmembrane domain affect the efficacy of these inhibitors, and such residues have been implicated in cation binding and transport by the protein (31). To determine the potential significance of the amino acids of TM VII in amiloride efficacy, we examined the effect of the mutations to alanine on the efficacy of the amiloride analog EMD87580. Initial experiments characterized the effect of EMD87580 on the wild type Na^+/H^+ exchanger expressed in AP-1 cells. An IC_{50} of 0.7 μM was obtained (not shown). We then did preliminary testing of the effect of this concentration of EMB87580 on all Na^+/H^+ exchanger mutants with enough activity (>30%) to be reproducibly measured. Several of the mutants displayed either increased (Ile^{251}, Val^{272}, and Leu^{273}) or decreased (Leu^{255} and Leu^{265}) resistance to EMD87580, whereas others were not different from the wild type (not shown). Those displaying altered sensitivity to EMD87580 were analyzed in further detail. The results are shown in Fig. 5. The

L265A and L255A mutants were more sensitive to inhibition (IC_{50} values, Leu^{265}, 0.08 μM; Leu^{255}, 0.28 μM) than the wild type (0.7 μM) Na^+/H^+ exchanger as was the Leu^{264} (IC_{50} 0.64 μM) mutant to a much smaller degree. In contrast the Val^{272} and Ile^{251} mutants were more resistant to EMD87580 (IC_{50}, Val^{272}, 3.6 μM; Ile^{251}, 2.2 μM), whereas the Leu^{273} mutant was slightly more resistant (IC_{50}, 1.8 μM) in comparison to the wild type.

Insertional Mutagenesis—Alanine insertional mutagenesis within a transmembrane segment has been used to scan membrane domains of lactose permease (16), the *Escherichia coli* F_1F_0-ATP synthase (32), and other proteins (33–35). Two mutants were made with alanine insertions. Alanines were inserted between amino acids 261 and 262 (Ins261A), and a different mutant had an alanine inserted between amino acids 264 and 265 (Ins264A). A third related mutant had asparagine 266 mutated to aspartic acid plus a glutamic acid inserted between amino acids 261 and 262 (N266DIns261E). The reasoning behind the mutation was that if the positions of acidic residues in TM VII were critical, an insertion of glutamic acid between Gly^{261} and Glu^{262} might conserve a required charge at this position. In addition, mutation of Asn^{266} to an aspartic acid might, in effect, result in replacement of Asp^{267} with an aspartic acid that is shifted into the same position that was formerly occupied by Asp^{267}. For all the insertional mutants, expression of the protein was greatly decreased (Fig. 2*D*). Expression was from 28 to 39% of the control levels. In addition, in all cases the majority of the protein expressed was as a deglycosylated 95-kDa protein. In the double mutant there was almost no 110-kDa protein, whereas in the insertions after amino acids 261 and 264 there was relatively more 110-kDa protein. The pattern of expression of mostly 95-kDa protein was similar to that obtained for substitution of Glu^{262} with alanine (Fig. 2*B*). Surface expression of the insertional mutants was also greatly compromised. Ins261A and the double mutant were both ~ 80% intracellular in location. The Ins264A mutant was ~60% intracellular.

The activity of insertional mutants was assayed as described for alanine scanning mutations. The Ins264A mutant was virtually totally inactive, even after correction for targeting and expression levels. The Ins261A mutant retained ~25% activity after corrections. Despite the apparent lack of expression of the 110-kDa protein, the double mutant (N266DIns261E) retained significantly more raw activity than either of the single insertional mutants. In addition, after correction for targeting and expression levels, the mutant was as active as the wild type.

Peptide Design and Conditions for NMR Spectroscopy—Pairs of cationic residues at the N and C termini of extremely hydrophobic peptides such as 24-mers of leucines have been shown to aid in peptide purification and handling (36). Therefore, we chose to add a pair of lysines to the C terminus of the sequence following Tyr^{274}. The N terminus of the segment was chosen to be the basic His^{250} residue, and we opted to keep a free N-terminal amine group; therefore, no additional cationic residues were added at the N terminus. Although there is no biological relevance to the numbering, the pair of lysine residues at the C terminus are referred to herein as Lys^{275} and Lys^{276}. A number of TM VII peptides were prepared, either by fusion in the GB1 system (13, 37) or by chemical synthesis. In the former case, the yield of purified peptide upon cyanogen bromide cleavage was extremely low. All high resolution structural studies were therefore carried out using two different synthetic peptides with identical sequences, one of which had no isotope labels and one selectively ^{15}N-labeled at residues Leu^{254}, Leu^{258}, Gly^{261}, Leu^{264}, Ala^{268}, and Leu^{273}.

A number of organic solvent conditions were initially tried as membrane mimetics for the TM VII peptides: a methanol/chloroform/water (4:4:1 v/v) mixture, dimethyl sulfoxide, acetonitrile, chloroform, and mixtures of acetonitrile and hexafluoropropanol. Note that the first two conditions were previously found to provide stable solubilization of the TM IV segment of NHE1 (13). SDS micelles (pH ~5) also failed to solubilize TM VII. In many cases, promising one-dimensional ^1H NMR spectra were obtained, but the peptide would come out of solution after ~4–24 h. These were generally precipitates that could be readily resuspended in solution, as opposed to irreversible aggregates. The same phenomenon was noticed in fractions containing the TM VII peptide collected during HPLC purification in 0.5% trifluoroacetic acid/isopropyl alcohol/water mixtures. Conversely, DPC micelles containing TM VII stayed in solution for weeks at ambient temperature. Sample components were ~1 mM peptide, ~75 mM deuterated DPC, and 1 mM 2,2-dimethyl-2-silapentane-5-sulfonic acid (as a chemical shift standard) in 90% H_2O, 10% D_2O adjusted to pH ~4.8 and studied at 30 °C. Note that this temperature is lower than temperatures often employed for DPC micelle studies, allowing use of the cryogenically cooled triple-resonance probe on the 800-MHz Canadian National High Field NMR Centre spectrometer but still providing extended stability of the samples and retention of good spectral characteristics. This combination of factors allowed determination of the structure of TM VII in DPC micelles.

Resonance Assignment and Structure Calculation—Sequential chemical shift assignments were carried out using TOCSY experiments, including ^{15}N-edited three-dimensional ^1H-^{15}N TOCSY-HSQC experiments for the isotope-labeled TM VII peptide, natural abundance ^1H-^{13}C HSQC experiments, and two-dimensional NOESY experiments (38, 39). Natural abundance ^1H-^{15}N HSQC was not feasible because of low signal-to-noise arising from the tumbling rate of the TM VII micelles. Poor coherence transfer from H^N protons, characteristic of $J_{HN\alpha}$ in α-helices (40), made TOCSY and ^{15}N-edited experiments less efficient and full unambiguous assignment difficult because of H^α overlap. Despite these difficulties, we were able to unambiguously assign all backbone H^N and H^α resonances (excluding the N-terminal NH_3^+) and the vast majority of side chain protons. (Unambiguous assignment of all Leu H^β and H^γ resonances was not possible; ambiguous NOE assignments were frequently employed in these cases.) Coupling from ^{15}N nuclei in the labeled sample in the either the indirect or both dimensions served to aid in assignment of ambiguous ^1H resonances. C^α and C^β (where applicable) chemical shifts were also assigned for all residues. Resonance assignments have been deposited in the BioMagResBank.

NOE build-up experiments carried out at 500 MHz over the range of mixing times from 75 to 350 ms indicated an optimal

TABLE 2
NMR structural statistics for the final ensemble of 33 pairs of structures retained out of 60 pairs calculated

Unique NOE restraints	
Total	1311
Intra-residue	381
Sequential	373
Medium range ($\|i-j\| \leq 4$)	398
Long range ($\|i-j\| > 4$)	23
Ambiguous	136
Ramachandran plot statistics	
Core	63.2%
Allowed	34.6%
Generously allowed	2.0%
Disallowed	0.3%
XPLOR-NIH energies (kcal/mol)[a]	
Total	51.0 ± 4.8
NOE	5.11 ± 1.4
NOE violations	
Violations >0.5 Å	0
Violations of 0.3–0.5 Å	1
Violations of 0.2–0.3 Å	4

[a] Note that energy given is for a pair of structures calculated as described.

mixing time of 225–250 ms (results not shown). ^{1}H-^{1}H NOE restraints were assigned using homonuclear spectra acquired at 800 MHz and pooled for the unlabeled and ^{15}N-selective labeled samples. As with resonance assignment, comparison of ^{15}N-^{1}H coupled *versus* decoupled spectra with the ^{15}N-labeled sample proved extremely useful in assignment of some ambiguous restraints. As detailed in the Supplemental Material, structure calculation made use of pairs of TM VII polypeptides. Each inter-residue restraint was made ambiguous, in that it could be satisfied either within a given polypeptide chain or between chains. Furthermore, through distance averaging any restraint could be satisfied in a single conformer or through dimerization. After refinement, a total of 1311 unique NOE restraints (Table 2) were used for calculation of the two-conformer TM VII structure. These are summarized graphically in terms of the standard connectivities examined for secondary structure characterization and in terms of the number of unique restraints per residue in Fig. 6. Chemical shift analysis indicates a negative deviation for H^{α} from random coil over residues Asn^{252}–Lys^{276} alongside a positive deviation from random coil for C^{α} and a negative deviation for C^{β} over residues His^{250}–Lys^{275}, as illustrated in Fig. 7 (random coil values from Ref. 41). Deviation of H^N chemical shift from temperature-corrected (42) random coil shifts (41) displays a periodic character over 4–5-residue stretches, and actual chemical shifts show a general upfield shift from the N to C terminus (not shown). As a whole, chemical shift data over residues Asn^{252}–Lys^{275} for H^{α}, C^{α}, and C^{β} (43) and for H^N (44, 45) are strongly indicative of α-helical secondary structure, including surpassing the chemical shift index cutoffs (*dashed lines* in Fig. 7, *A* and *B*) for both H^{α} (46) and C^{α} (47). Therefore, restraints of $\phi = -60 \pm 30$ and $\varphi = -40 \pm 40$ were included over residues Asn^{252}–Lys^{275}, where all chemical shifts differences relative to random coil and H^N periodicity characteristics indicated helical character. Hydrogen bond restraints were not employed as we feel that these would too strongly bias the structure toward an ideal α-helix rather than allowing combined satisfaction of the dihedral angles indicated by chemical shift data and of the observed NOE restraints. NOE restraint violations in the final ensemble of 66 retained structures are given in Table 2, and a Ramachandran plot for the ensemble of retained structures demonstrating the general agreement with ϕ and φ restraints is shown in Fig. 8.

DISCUSSION

Functional Analysis of TM VII—Transmembrane segment VII is critical for the function of NHE1. We earlier demonstrated that Glu^{262} and Asp^{267} are critical for activity, with negative charges at these positions being crucial for function (14). We used alanine scanning mutagenesis (48, 49) and replaced all amino acids of TM VII. Alanine is a small, hydrophobic, helix-forming amino acid that is relatively nonintrusive (15). We also used alanine insertional mutagenesis. Insertion of an alanine within a transmembrane segment has been used to scan membrane domains of the lactose permease (16), the *E. coli* F_1F_0-ATP synthase (32), glycophorin A (35), and other proteins. Insertion of a single amino acid into a transmembrane helix displaces residues by 110° relative to other residues. This can disrupt helix-helix packing interfaces and can shift the location of critical residues involved in either cation binding and transport or helix-helix interactions (35). The effect of alanine insertions is specific and varies from protein to protein and TM segment to TM segment (34).

Initial experiments substituted each of the amino acids of TM VII with alanine residues. Alanine 268 was left unchanged. We found that mutation to alanine caused varying effects on NHE1 activity and expression and targeting. Between amino acids 255 and 262 most mutants lost ~50% of their activity. The effect on activity of mutant Glu^{262}, Leu^{254}, Leu^{255}, Val^{269}, and Leu^{273} was accounted for, in part, by effects on targeting and expression levels. For mutant E262A, we observed that a large portion of the protein was present as a partial or de-glycosylated form. This correlated with aberrant targeting of the protein, which we have seen earlier in NHE1 (12, 13). Mutations to amino acids 266 and 267 resulted in mostly inactive protein, even after correcting for expression and targeting. We previously showed that a negative charge at amino acid 267 is critical for activity. Mutation of this residue to Asn caused loss of activity, whereas mutation to Glu retained normal activity (14). Our present results confirm this observation and show that the smaller Ala residue also cannot substitute for a charged amino acid.

Although we found many cases of reduced activity of NHE1 via substitution with Ala, including residues Leu^{254}, Leu^{255}, His^{256}, Ile^{257}, Val^{259}, Phe^{260}, Gly^{261}, Glu^{262}, Asn^{266}, Asp^{267}, Thr^{270}, Val^{271}, and Val^{272}, there were actually few residues in which activity was extremely reduced. This is in contrast to what was observed earlier with TM IV, in which substitution to Cys results in a nearly inactive protein in many cases. The difference between these results could be due to a difference in the transmembrane segments themselves. For example TM XI of the lactose permease was very sensitive to mutation (50), whereas TM XII was not (51). However, in this study, the replacements in TM VII of NHE1 were done with Ala as opposed to Cys replacements of TM IV in our earlier study (13). As this segment was found to be predominantly helical in character, small helix-forming alanine may be less disruptive in this

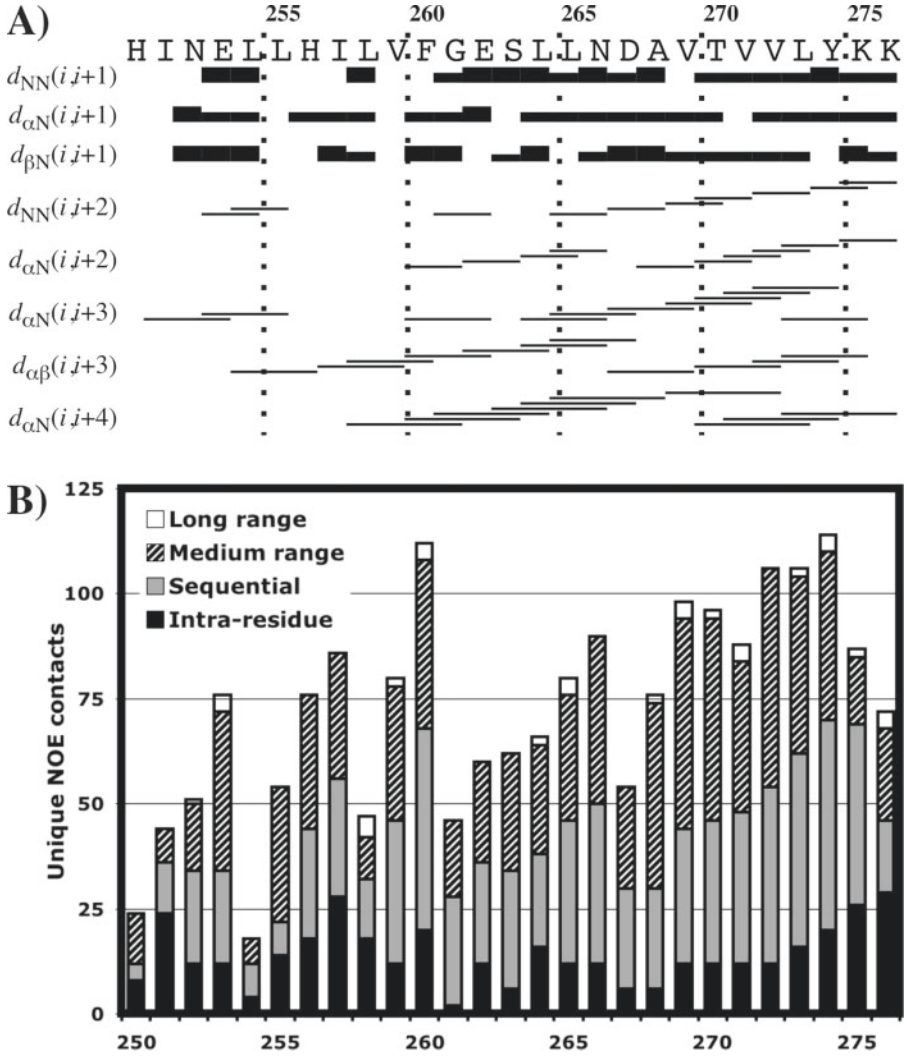

FIGURE 6. **NOE restraint assignments for TM VII in DPC micelles.** *A,* graphical summary of d_{xx} NOE restraints observed in homonuclear NOESY experiments. (Figure was modified from CYANA (L.A. Systems, Inc.) output.) *B,* number of unique NOE restraints in final set of restraints on a per-residue basis (medium range restraints are between nuclei 2 and 4 residues apart in sequence; long range are 5 or more residues apart).

transmembrane segment than a Cys residue was in TM IV (13). Alanine may better preserve the overall character of TM VII and be a better choice for examining the importance of side chains and helical character, as compared with insertion of a Cys residue because Cys has a much lower propensity than Ala for α-helix formation in a TM region (52, 53). The results suggest that many of the side chains of the amino acids do not appear to be especially critical for activity, although they sometimes influenced expression levels and targeting. When considering corrections for expression levels and targeting, the subgroup that had activity reduced 50% or more included only Leu^{255}, Ile^{257}, Val^{259}, Phe^{260}, Gly^{261}, Asn^{266}, Asp^{267}, and Thr^{270}. The E262A mutation caused a very large decrease in activity, although much of this was because of aberrant targeting and expression, and after these corrections activity was slightly over 50% of control.

Alanine insertional mutagenesis suggested that the overall structure of TM VII was critical. Insertion of Ala after either amino acid 261 or 264 resulted in an almost completely inactive protein. Because of the importance of amino acid Asp^{267}, we reasoned that if we inserted a glutamic acid after amino acid 261, on the initial assumption of an ideal α-helix, the helix might shift such that amino acid Asn^{266} was in the position of Asp^{267}. Mutation of Asn^{266} to Asp might return a critical acidic residue to this position. In addition, the glutamic acid insertion after Gly^{261} might substitute for Glu^{262}. In fact, we found that this double mutant retained much more activity than simple insertion of alanine after 261. Upon correction for defective targeting and expression, the activity was equivalent to that of the controls (Fig. 4*B*). This was somewhat surprising because the protein was even more poorly glycosylated than the other insertional mutants (Fig. 2*D*); however, we have previously shown that glycosylation is not essential to NHE1 function (29). Although having two glutamate residues following one another in the mutant would not be conducive to α-helix formation (52, 54), this region is extended rather than helical in the structure of TM VII that we have solved.

An important characteristic of the NHE1 protein is its sensitivity to inhibition by benzoyl guanidine type of inhibitors. Sites in TM IV (55) and TM IX (56–58) alter sensitivity to inhibition. We reasoned that because of the critical nature of this transmembrane segment, it might also affect sensitivity to inhibition. Several of the residues altered the sensitivity. The maximum changes were a 10-fold increase in sensitivity to inhibition with mutation of L265A and a 5-fold increase in resistance with the V272A mutation. These changes are not as large as some reported earlier (58), but nonetheless they altered the inhibitor efficacy significantly. Other mutations have reported significant effects on NHE inhibitor resistance but no effects on Na^+ affinity (59), suggesting that the inhibitor-binding site may be physically distinct but closely related to the Na^+-binding site (60). The contribution of many regions of the NHE1 protein to inhibitor resistance, shown in this and other studies, suggests that a number of different regions of the protein likely come together to influence the protein structure and thereby influence the NHE inhibitor-binding site. Likely, alterations in many amino acids and transmembrane segments that affect the structure and function of the protein affect inhibitor binding. However, we did find that the effects were specific. Amino acids Leu^{265}, Leu^{255}, Ile^{251}, and Val^{272} had significant effects on NHE1 inhibitor resistance whereas others did not.

Structural Analysis of TM VII—Attempts to calculate a single conformer in agreement with the assigned NOE data required removal of a high proportion (34.4%) of the NOE restraint data to allow production of an ensemble of structures with low violation statistics (data not shown). Two possible reasons for the inability to satisfy the NMR data were that the TM VII peptide was sampling a number of conformations, as is frequently observed with peptides or unstructured proteins, or that oligomerization of the TM VI peptide was taking place. In either case, NOE restraints would be observed that are not satisfied by a single conformation. Interestingly, we found that simultaneous calculation of two conformers satisfied the NOE data set without significant dimer formation suggesting that sampling of multiple conformations rather than dimerization is responsible for reducing restraint violations. A similar result, but without the ability to test for dimerization, could likely be achieved through ensemble-average structure calculation (61–64). Further details are supplied in the Supplemental Material.

An ensemble of 66 TM VII structures (33 dual conformer pairs) was obtained that satisfy the vast majority of observed NOE and chemical shift-derived ϕ and ψ dihedral angle restraints equally well (Table 2; Fig. 8). Despite strong chemical shift evidence (Fig. 7; values deposited in the BioMagResBank), NOE connectivities (Table 2 and Fig. 6; restraints deposited in the Protein Data Bank code 2HTG and RCSB code RCSB038740) do not result in an uninterrupted helix over residues Asn^{252}–Lys^{275}. Superposition of all members of the ensemble over the full length of the peptide is not possible. Rather, two distinct portions of the peptide show strong structural convergence, as demonstrated by superposition of the polypeptide backbone over the ensemble of structures. The break point between these converged segments of TM VII is at Gly^{261}–Glu^{262}. Minor variability in backbone structure is also observed over the ensemble of structures at Leu^{254}–Leu^{255}, Leu^{265}–Asn^{266}, and Thr^{270}–Val^{271}, requiring separate superpositions for optimal root mean square deviation, as detailed in the Supplemental Material. Residues highlighted in *gray* in Fig. 8 with greater than usual dispersion of (ϕ,ψ) angle are Ile^{251} (corresponding to flexibility at the N terminus), Gly^{261} (corresponding to major break between helical segments), and Val^{271} (corresponding to minor variability in positioning of the C terminus relative to N terminus of helical segment ~Ser^{264}–Leu^{273}). Using the Kabsch-Sander secondary structure assignment method (65) as implemented in PROMOTIF (66), helical structure predominates over the converged segments N- and C-terminal to Gly^{261}. In the N terminus, helical structure predominates from Leu^{255}–Phe^{260} and in the C terminus from Leu^{264}–Val^{272} (detailed analysis in the Supplemental Material). In a given two-conformer structure in agreement with the experimental data, the relative positions and orientations of the two helical segments about Gly^{261}–Glu^{262} tend to differ.

The structure of TM VII in DPC micelles is therefore an interrupted helix. A representative conformer from the ensemble of structures is shown in Fig. 9. The relative positioning and orientation of the N- and C-terminal helical stretches are quite variable about Gly^{261} in the isolated TM segment. However, in the protein environment this would likely be a well defined kink, with strong potential for an interruption in helicity over

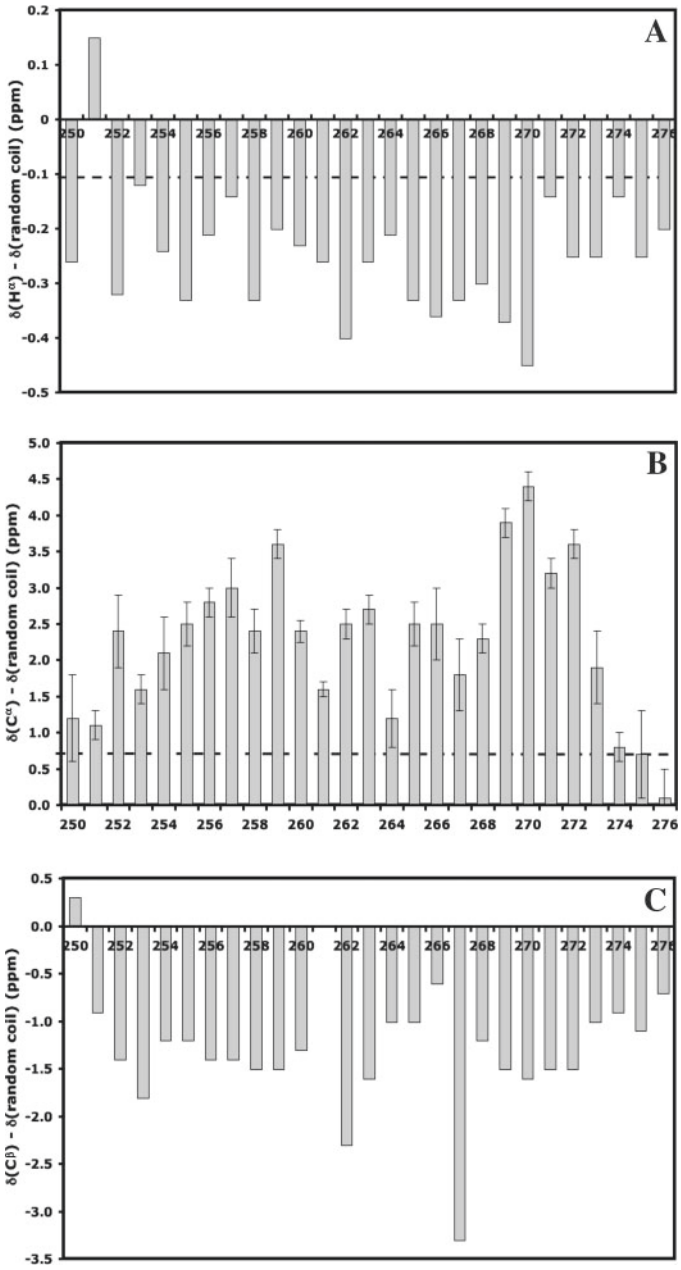

FIGURE 7. **Chemical shifts for TM VII in DPC micelles.** Chemical shift differences from random coil shifts (41) are shown for H^{α} (*A*), C^{α} (*B*), and C^{β} (*C*). *Dashed lines* in *A* and *B* are chemical shift difference cutoffs considered significant for the ^{1}H (46) and ^{13}C (47) chemical shift indices, respectively.

the range Phe^{260}–Ser^{263}. It should be noted that in the prokaryotic Na^{+}/H^{+} exchanger NhaA (67), as well as a number of other membrane protein structures, kinked and interrupted helices are thought to play crucial roles in function. The inherent flexibility of the TM VII segment about Gly^{261} also suggests the potential for structural change in response to pH, as has been hypothesized to be take place with the kinked and interrupted helical transmembrane segments IV and XI of NhaA (67). The exact role of TM VII in ion transport should become more apparent as the pH sensor mechanism of NHE1 becomes better understood.

Correlating Structural and Functional Data—There are interesting correlations between the structural and functional

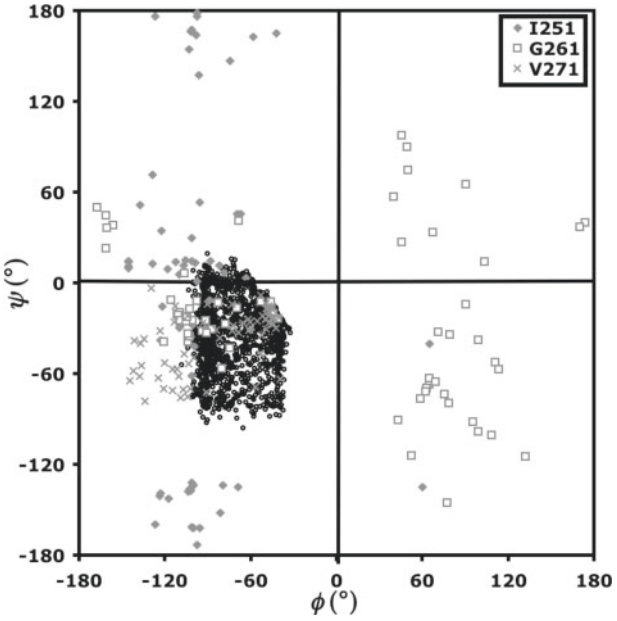

FIGURE 8. **Ramachandran plot for entire retained ensemble of TM VII peptide structures.** Residues Ile^{251}, Gly^{261}, and Val^{271} are shown in *gray* as indicated; all other residues over the range Asn^{252}–Lys^{276} are shown as *open black circles*.

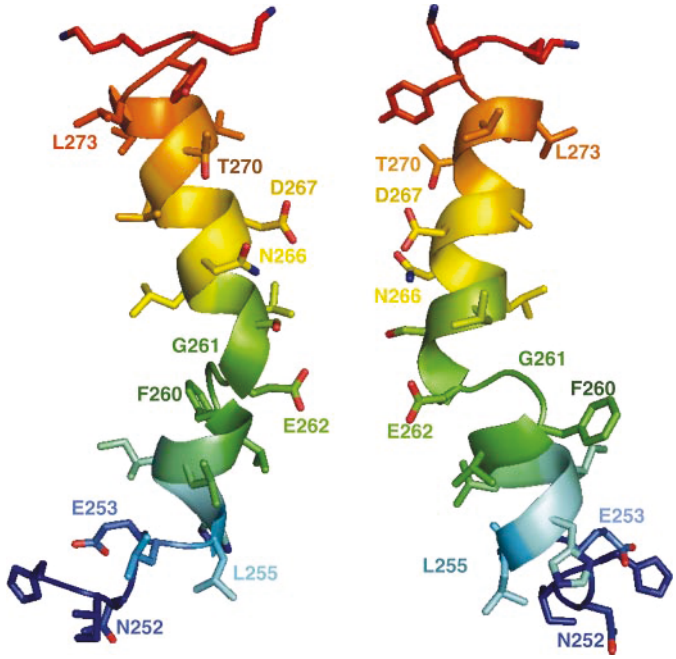

FIGURE 9. **Representative structure of TM VII peptide.** Two different orientations of a representative ensemble member are shown side-by-side with coloring covering the spectrum from *blue* (N terminus) to *red* (C terminus). The ensemble of structures shows a variety of orientations of the N- and C-terminal α-helical segments about Gly^{261}; side chain positions are also typically variable.

data. One of the key areas of sensitivity to mutation was at amino acids Gly^{261} and Glu^{262} where we observed a strong break in helical structure. For Glu^{262}, we earlier showed that the conservative mutation to Asp allowed retention of most of the normal properties of the protein, whereas switching to uncharged Asn resulted in a dysfunctional protein (14). The helix-breaking nature of the GE pair of residues would likely be retained in both of these mutants (52, 54), giving further evidence that it is the acidic functionality of Glu^{262} that is crucial to NHE1 activity. The insertion of an Ala between Gly^{261} and Glu^{262} also disrupts NHE1 activity, implying that both the position of Glu^{262} and the nonhelical nature of the Gly^{261}–Glu^{262} region are crucial. The ability of the Gly^{261}–Ser^{263}/Leu^{264} region to undergo conformational change, reflected by variability about this region in the TM VII structure, may also be functionally crucial because the F260A, G261A, and E262A mutants would all increase the helical propensity of this region, and all are highly disruptive to function.

In converse to these residues, the activity of NHE1 is insensitive to the S263A mutant. Ser^{263} shows more involvement in the helix at the C terminus of TM VII than would be expected based upon helical propensities. The helical character of residue 263 would be strengthened in the S263A mutant. Ser is also proposed to have a strong propensity for allowing close packing of TM helices. If this were its role, a Ser → Ala mutant is actually highly conservative because Ala and Ser have very similar packing characteristics (68). Replacement of the subsequent Leu^{264} or Leu^{265} with Ala did not greatly inhibit activity, after correction for expression and targeting was taken into account. Therefore, it seems that the local structure rather than the chemical character of side chains over Ser^{263}–Leu^{265} is important for function, with the good possibility that substitution of Ser^{263} with a residue of lower helical packing capability would affect overall NHE1 structure.

Substitution of Asn^{266}, Asp^{267}, or Thr^{270} with alanine inactivated NHE1. The negatively charged side chain of Asp^{267} is critical to activity, because even the conservative D267N mutant results in loss of activity (14). The α-helical nature of the TM VII segment over the range including Asn^{266}, Asp^{267}, and Thr^{270} means that all three side chains fall on the same face of the segment (for example see their positions in Fig. 9). Negatively charged amino acids have been reported to be present in the funnel region of the prokaryotic Na^+/H^+ exchanger NhaA (67), and Asp^{267} could play a similar role in NHE1. Along these lines, Thr^{270} may have an analogous function to Thr^{132} of NhaA, which serves an important, although not essential, role in Na^+ binding (67). Therefore, it is possible that the side chains of these three residues are all involved in a cytoplasmic side ion funnel of NHE1 similar to that proposed for NhaA. Alternatively, the Asp^{267} side chain may form a critical salt bridge for functional protein structure. As with Ser, Thr is proposed to allow close packing of TM segments in membranes (68), meaning that Thr^{270} may readily have a crucial packing interaction with the same neighboring segment that would be disrupted by replacement with the much smaller Ala side chain. Insertion of an Ala between Leu^{264} and Leu^{265} would disrupt either role of these critical residues by shifting the register of the entire helix off by one residue, and this insertional mutant indeed showed strongly perturbed expression, targeting, and activity.

Our study gives a detailed structural and full functional picture of TM VII. TM VII is a transmembrane segment that is critical for NHE1 function. We demonstrate that 13 of 22 residues were sensitive to mutation to alanine and that

mutation of 5 residues altered sensitivity to inhibition by EMD87580. In contrast to TM IV of NHE1, TM VII is predominantly α-helical. However, it has a pronounced break in helicity in its central region, which includes the functionally essential acidic Glu^{262} residue. The helical nature of the C terminus of this segment positions three critical residues (Asn^{266}, Asp^{267}, and Thr^{270}) on the same face of the segment. If these are determined to be involved in ion transport rather than structural stabilization of NHE1, this result provides a starting point for mechanistic elucidation of ion funneling and transport. Future experiments may both further elaborate the role of TM VII in ion exchange and examine the structure-function relationship for other TM segments of the NHE1 isoform of the Na^+/H^+ exchanger.

Acknowledgments—We thank Jeffrey DeVries for maintenance of the 500-MHz Varian Inova spectrometer; Jason Moses and Marc Genest of the Protein Engineering Network of Centres of Excellence Chemistry Laboratory in Edmonton, Alberta, Canada, for synthesis, purification, and characterization of peptides; Charles Schwieters from the National Institutes of Health (Bethesda) for helpful discussions regarding XPLOR-NIH; and the Canadian National High Field NMR Centre for their assistance and use of their facilities. Peptide synthesis, NMR spectroscopy, and structural calculations were funded by Protein Engineering Network of Centres of Excellence. Operation of Canadian National High Field NMR Centre is funded by Canadian Institutes of Health Research, Natural Sciences and Engineering Research Council of Canada, and the University of Alberta.

REFERENCES

1. Orlowski, J., and Grinstein, S. (1997) *J. Biol. Chem.* **272,** 22373–22376
2. Grinstein, S., Rotin, D., and Mason, M. J. (1989) *Biochim. Biophys. Acta* **988,** 73–97
3. Pouyssegur, J., Sardet, C., Franchi, A., L'Allemain, G., and Paris, S. (1984) *Proc. Natl. Acad. Sci. U. S. A.* **81,** 4833–4837
4. Shrode, L., Cabado, A., Goss, G., and Grinstein, S. (1996) in *The Na^+/H^+ Exchanger* (Fliegel, L., ed) pp. 101–122, R. G. Landes Co., Austin, TX
5. Karmazyn, M., Liu, Q., Gan, X. T., Brix, B. J., and Fliegel, L. (2003) *Hypertension* **42,** 1171–1176
6. Fliegel, L. (2001) *Basic Res. Cardiol.* **96,** 301–305
7. Mentzer, R. M., Jr., Lasley, R. D., Jessel, A., and Karmazyn, M. (2003) *Ann. Thorac. Surg.* **75,** S700–S708
8. Lang, H. J. (2003) in *The Na^+/H^+ Exchanger, From Molecular to Its Role in Disease* (Karmazyn, M., Avkiran, M., and Fliegel, L., eds) pp. 239–253, Kluwer Academic Publishers, Norwell, MA
9. Paradiso, A., Cardone, R. A., Bellizzi, A., Bagorda, A., Guerra, L., Tommasino, M., Casavola, V., and Reshkin, S. J. (2004) *Breast Cancer Res.* **6,** R616–R628
10. Denker, S. P., and Barber, D. L. (2002) *J. Cell Biol.* **159,** 1087–1096
11. Wakabayashi, S., Pang, T., Su, X., and Shigekawa, M. (2000) *J. Biol. Chem.* **275,** 7942–7949
12. Slepkov, E. R., Chow, S., Lemieux, M. J., and Fliegel, L. (2004) *Biochem. J.* **379,** 31–38
13. Slepkov, E. R., Rainey, J. K., Li, X., Liu, Y., Cheng, F. J., Lindhout, D. A., Sykes, B. D., and Fliegel, L. (2005) *J. Biol. Chem.* **280,** 17863–17872
14. Murtazina, B., Booth, B. J., Bullis, B. L., Singh, D. N., and Fliegel, L. (2001) *Eur. J. Biochem.* **268,** 1–13
15. Fleming, K. G., and Engelman, D. M. (2001) *Proc. Natl. Acad. Sci. U. S. A.* **98,** 14340–14344
16. Braun, P., Persson, B., Kaback, H. R., and von Heijne, G. (1997) *J. Biol. Chem.* **272,** 29566–29571
17. Oblatt-Montal, M., Reddy, G. L., Iwamoto, T., Tomich, J. M., and Montal, M. (1994) *Proc. Natl. Acad. Sci. U. S. A.* **91,** 1495–1499
18. Wigley, W. C., Vijayakumar, S., Jones, J. D., Slaughter, C., and Thomas, P. J. (1998) *Biochemistry* **37,** 844–853
19. Hunt, J. F., Earnest, T. N., Bousche, O., Kalghatgi, K., Reilly, K., Horvath, C., Rothschild, K. J., and Engelman, D. M. (1997) *Biochemistry* **36,** 15156–15176
20. Katragadda, M., Alderfer, J. L., and Yeagle, P. L. (2001) *Biophys. J.* **81,** 1029–1036
21. Katragadda, M., Chopra, A., Bennett, M., Alderfer, J. L., Yeagle, P. L., and Albert, A. D. (2001) *J. Pept. Res.* **58,** 79–89
22. Naider, F., Khare, S., Arshava, B., Severino, B., Russo, J., and Becker, J. M. (2005) *Biopolymers* **80,** 199–213
23. Damberg, P., Jarvet, J., and Graslund, A. (2001) *Methods Enzymol.* **339,** 271–285
24. Henry, G. D., and Sykes, B. D. (1994) *Methods Enzymol.* **239,** 515–535
25. Zhang, Y. P., Lewis, R. N., Hodges, R. S., and McElhaney, R. N. (1995) *Biophys. J.* **68,** 847–857
26. Wishart, D. S., Bigam, C. G., Yao, J., Abildgaard, F., Dyson, H. J., Oldfield, E., Markley, J. L., and Sykes, B. D. (1995) *J. Biomol. NMR* **6,** 135–140
27. Delaglio, F., Grzesiek, S., Vuister, G. W., Zhu, G., Pfeifer, J., and Bax, A. (1995) *J. Biomol. NMR* **6,** 277–293
28. Schwieters, C. D., Kuszewski, J. J., Tjandra, N., and Clore, G. M. (2003) *J. Magn. Reson.* **160,** 65–73
29. Haworth, R. S., Frohlich, O., and Fliegel, L. (1993) *Biochem. J.* **289,** 637–640
30. Li, X., Ding, J., Liu, Y., Brix, B. J., and Fliegel, L. (2004) *Biochemistry* **43,** 16477–16486
31. Karmazyn, M., Sawyer, M., and Fliegel, L. (2005) *Curr. Drug Targets Cardiovasc. Haematol. Disord.* **5,** 323–335
32. Vik, S. B., Patterson, A. R., and Antonio, B. J. (1998) *J. Biol. Chem.* **273,** 16229–16234
33. Op De Beeck, A., Montserret, R., Duvet, S., Cocquerel, L., Cacan, R., Barberot, B., Le Maire, M., Penin, F., and Dubuisson, J. (2000) *J. Biol. Chem.* **275,** 31428–31437
34. Op De Beeck, A., Molenkamp, R., Caron, M., Ben Younes, A., Bredenbeek, P., and Dubuisson, J. (2003) *J. Virol.* **77,** 813–820
35. Mingarro, I., Whitley, P., Lemmon, M. A., and von Heijne, G. (1996) *Protein Sci.* **5,** 1339–1341
36. Davis, J. H., Clare, D. M., Hodges, R. S., and Bloom, M. (1983) *Biochemistry* **22,** 5298–5305
37. Lindhout, D. A., Thiessen, A., Schieve, D., and Sykes, B. D. (2003) *Protein Sci.* **12,** 1786–1791
38. Cavanagh, J., Fairbrother, W., Palmer, A. G., III, and Skelton, N. J. (1996) *Protein NMR Spectroscopy: Principles and Practice*, Academic Press, New York
39. Wuthrich, K. (1986) *NMR of Proteins and Nucleic Acids*, Wiley Interscience, New York
40. Cavanagh, J., Chazin, W. J., and Rance, M. (1990) *J. Magn. Reson.* **87,** 110–131
41. Wishart, D. S., Bigam, C. G., Holm, A., Hodges, R. S., and Sykes, B. D. (1995) *J. Biomol. NMR* **5,** 67–81
42. Merutka, G., Dyson, H. J., and Wright, P. E. (1995) *J. Biomol. NMR* **5,** 14–24
43. Wishart, D. S., Sykes, B. D., and Richards, F. M. (1991) *J. Mol. Biol.* **222,** 311–333
44. Kuntz, I. D., Kosen, P. A., and Craig, E. C. (1991) *J. Am. Chem. Soc.* **113,** 1406–1408
45. Williamson, M. P. (1990) *Biopolymers* **29,** 1423–1431
46. Wishart, D. S., Sykes, B. D., and Richards, F. M. (1992) *Biochemistry* **31,** 1647–1651
47. Wishart, D. S., and Sykes, B. D. (1994) *J. Biomol. NMR* **4,** 171–180
48. Lu, Z. L., Saldanha, J. W., and Hulme, E. C. (2001) *J. Biol. Chem.* **276,** 34098–34104
49. Fraysse, A. S., Moller, A. L., Poulsen, L. R., Wollenweber, B., Buch-Pedersen, M. J., and Palmgren, M. G. (2005) *J. Biol. Chem.* **280,** 21785–21790
50. Dunten, R. L., Sahin-Toth, M., and Kaback, H. R. (1993) *Biochemistry* **32,** 12644–12650
51. He, M. M., Sun, J., and Kaback, H. R. (1996) *Biochemistry* **35,** 12909–12914

52. Jones, D. T., Taylor, W. R., and Thornton, J. M. (1994) *Biochemistry* **33,** 3038–3049
53. Liu, H., Cala, P. M., and Anderson, S. E. (1998) *J. Mol. Cell. Cardiol.* **30,** 685–697
54. Liu, L. P., and Deber, C. M. (1998) *J. Biol. Chem.* **273,** 23645–23648
55. Counillon, L., Franchi, A., and Pouyssegur, J. (1993) *Proc. Natl. Acad. Sci. U. S. A.* **90,** 4508–4512
56. Khadilkar, A., Iannuzzi, P., and Orlowski, J. (2001) *J. Biol. Chem.* **276,** 43792–43800
57. Orlowski, J., and Kandasamy, R. A. (1996) *J. Biol. Chem.* **271,** 19922–19927
58. Noel, J., Germain, D., and Vadnais, J. (2003) *Biochemistry* **42,** 15361–15368
59. Wang, D., Balkovetz, D. F., and Warnock, D. G. (1995) *Am. J. Physiol.* **269,** C392–C402
60. Harris, C., and Fliegel, L. (1999) *Int. J. Mol. Med.* **3,** 315–321
61. Bonvin, A. M., and Brunger, A. T. (1995) *J. Mol. Biol.* **250,** 80–93
62. Bonvin, A. M. J. J., Boelens, R., and Kaptein, R. (1994) *J. Biomol. NMR* **4,** 143–149
63. Bruschweiler, R., Blackledge, M., and Ernst, R. R. (1991) *J. Biomol. NMR* **1,** 3–11
64. Wang, J. J., Hodges, R. S., and Sykes, B. D. (1995) *J. Am. Chem. Soc.* **117,** 8627–8634
65. Kabsch, W., and Sander, C. (1983) *Biopolymers* **22,** 2577–2637
66. Hutchinson, E. G., and Thornton, J. M. (1996) *Protein Sci.* **5,** 212–220
67. Hunte, C., Screpanti, E., Venturi, M., Rimon, A., Padan, E., and Michel, H. (2005) *Nature* **435,** 1197–1202
68. Eilers, M., Shekar, S. C., Shieh, T., Smith, S. O., and Fleming, P. J. (2000) *Proc. Natl. Acad. Sci. U. S. A.* **97,** 5796–5801

Structural and Functional Characterization of Transmembrane Segment VII of the Na^+/H^+ Exchanger Isoform 1

Jie Ding, Jan K. Rainey, Caroline Xu, Brian D. Sykes and Larry Fliegel

J. Biol. Chem. 2006, 281:29817-29829.
doi: 10.1074/jbc.M606152200 originally published online July 21, 2006

Supplementary material to:

"Structural and Functional Characterization of TM VII of the NHE1 isoform of the Na^+/H^+ exchanger" by Ding, Rainey, Xu, Sykes & Fliegel. *J. Biol. Chem.*

Details of dual-conformer structure calculation

Attempts to calculate a single conformer structure in agreement with the assigned NOE data required significant pruning of the restraints to allow production of an ensemble of structures with low violation statistics (data not shown). Pruning led to a total of 860/1311 retained unambiguous restraints, meaning that a high proportion (34.4%) of the NOE data had to be discarded. Two possible reasons for the inability to satisfy the NMR data were that the TM VII peptide was sampling a number of conformations, as is frequently observed with peptides or unstructured proteins, or that oligomerization of the TM VI peptide was taking place. In either case, NOE restraints would be observed which are not satisfied by a single conformation.

In order to test for oligomerization without excluding the multiple-conformer case, we carried out structure calculations where each inter-residue NOE restraint was made ambiguous, with calculations carried out using two identical polypeptides (termed chains A and B). For example, a restraint between atom 1 and atom 2 would be satisfied by an appropriate r^6 summed and averaged distance for the four distances: (i) between chain A-atom 1 and chain A-atom 2 (intra-polypeptide), (ii) chain B-atom 1 and chain B-atom 2 (intra-polypeptide), (iii) chain A-atom 1 and chain B-atom 2 (inter-polypeptide), and, (iv) chain B-atom 1 and chain A-atom 2 (inter-polypeptide). Because any given restraint could be satisfied through ^1H-^1H distances arising from dimerization (cases iii and iv) and also through distances observed within either or both of the individual polypeptide chains (cases i and/or ii), the calculation is not biased towards either the monomer or dimer state.

Interestingly, we found that simultaneous calculation of 2 conformers satisfied the NOE data set without significant dimer formation. 22/33 paired conformers had inter-chain atom-to-atom distances satisfying an average of only ~ 0.75% of NOE restraints (restraint numbers and classes given in Table II of the accompanying article). Such minimal observation of inter-chain ^1H-^1H restraint satisfaction suggests that sampling of

multiple conformations rather than dimerization is responsible for reducing restraint violations. A similar result, but without the ability to test for dimerization, could likely be achieved through ensemble-average structure calculation (1-4). Effectively, our result demonstrates that an "ensemble" of 2 conformers is sufficient at any given time to satisfy all observed (time-averaged) restraint data in the case of the TM VII peptide in DPC micelles. The final ensemble of retained structures is composed of a variety of conformers which show differences at flexible points in the structure, rather than of two distinct conformers.

Details of structure and superposition regions

Using the Kabsch-Sander secondary structure assignment method (5) as implemented in PROMOTIF (6), helical structure predominates over the converged segments N- and C-terminal to G261. In the N-terminal, helical structure predominates from L255-F260; in the C-terminal, from L264-V272. Actual assignment proportions of helical vs. H-bonded turns vary from ~50-87% of the ensemble, with central cores of the segments demonstrating a higher proportion of helical vs. turn assignment. A significant proportion of structures also show helical character at residues E253 (27 of 66 structures), L254 (32/66), G261 (25/66), E262 (30/66), S263 (31/66), and L273 (25/66). Good backbone RMSD convergence statistics imply that helicity is echoed even where formal secondary structure assignments are less clear (Fig. S1). Supporting these observations, the majority of residues over N252-K275 tend to cluster within the region of the Ramachandran plot given by $\phi \sim -60\pm30$ and $\varphi \sim -40\pm40$ (Fig. 8, accompanying paper), corresponding to the dihedral angle restraints placed upon these residues during simulated annealing. Residues highlighted in grey in Fig. 8 (see accompanying paper) with greater than usual dispersion of (ϕ,ψ) angle are I251 (corresponding to flexibility at the N-terminus), G261 (corresponding to major break between helical segments) and V271 (corresponding to minor variability in positioning of the C-terminus relative to N-terminus of helical segment ~S264-L273). Therefore, we believe the structure of TM-VII to be α-helical from E253 or L254 to V272 or L273 with a kink, and probable interruption in helical character, at G261. It should be noted that we observed a greater proportion of 3_{10}:α-helical character at the N-terminal of the segment (E253-L255).

Whether this is echoed in the segment within NHE1 or an artifact in the micelle state is not clear. This structural uncertainty does not affect the present analysis.

Although there are two major structurally convergent stretches in the TM VII structure, in order to achieve optimal heavy atom RMSD's, four superpositions were carried out (Figs. S1 and S2). The best regions for superposition were chosen initially using the program NMRCORE (7) and then refined by an iterative procedure where the superposed region was varied until an optimal RMSD was observed. Superposition was by the method of Kabsch (8) as implemented in the LSQKAB software of the CCP4 suite (9). Note that although this is a similar analysis to that in our structure determination of the TM IV peptide of NHE1 (10), the actual structures of these TM segments are not similar.

The helical segment L255-F260 superposes well. As evinced by the sharp increase in RMSD at E253-L254 (Fig. S1 – segment ii), there is some flexibility of the N-terminal region relative to this helix (Fig. S2(b)). The N-terminal region from I251-L255 superposes well itself (Fig. S1 – segment i), demonstrating a converged H-bonded turn (Fig. S2(a)). The segment over E262-Y274 shows a strongly converged core α-helical structure with slight variability at its N- and C-termini. Because of this variability, as seen in Fig. S2(c)-(d), two separate superpositions provide optimal RMSD's for each residue of the overlapping stretches E262-V269 and D267-Y274 (Fig. S1 segments iii and iv, respectively). L255 has shows two distinct clusters of (ϕ,ψ) dihedral angles, which probably gives rise to the need for separate superpositions of segments i and ii (Fig. S2(a)-(b)). The sharp increase in RMSD at the break between helical segments ii and iii (Fig. S1) is echoed by large variability of the (ϕ,ψ) dihedral angle distribution for G261 (Fig. 8, accompanying paper). The ψ angle of F260 also shows greater than usual variation and its (ϕ ,φ) distribution is clustered unusually in comparison to other residues. As with L255 and F260, L265 demonstrates a clustered dihedral angle distribution, likely echoing the increase in RMSD (Fig. S1) seen immediately N-terminal to segment iv (Fig S2(d)). The variability in backbone structure observed at T270-V271 is highlighted by greater spread of the ϕ angle of V271 as compared to the remainder of residues (Fig. 8, accompanying paper), which likely gives rise to the increased RMSD (Fig. S1) C-terminal to segment iii (Fig.S2(c)). The representative structure shown in Fig. 9 of the

accompanying paper is shown in Fig. S2(e) to aid in putting the superpositions into the context of the structure as a whole.

References

1. Bonvin, A. M., and Brunger, A. T. (1995) *J Mol Biol* **250**, 80-93
2. Bonvin, A.M.J.J., Boelens, R., and Kaptein, R. (1994) *J Biomol NMR* **4**, 143-149
3. Bruschweiler, R., Blackledge, M., and Ernst, R. R. (1991) *J Biomol NMR* **1**, 3-11
4. Wang, J. J., Hodges, R. S., and Sykes, B. D. (1995) *J Am Chem Soc* **117**, 8627-8634
5. Kabsch, W., and Sander, C. (1983) *Biopolymers* **22**, 2577-2637
6. Hutchinson, E. G., and Thornton, J. M. (1996) *Protein Sci* **5**, 212-220
7. Kelley, L. A., Gardner, S. P., and Sutcliffe, M. J. (1997) *Protein Eng* **10**, 737-741
8. Kabsch, W. (1976) *Acta Crystallogr A* **32**, 922-923
9. Collaborative Computational Project, N. (1994) *Acta Crystallogr D* **50**, 760-763
10. Slepkov, E. R., Rainey, J. K., Li, X., Liu, Y., Cheng, F. J., Lindhout, D. A., Sykes, B. D., and Fliegel, L. (2005) *J Biol Chem* **280**, 17863-17872

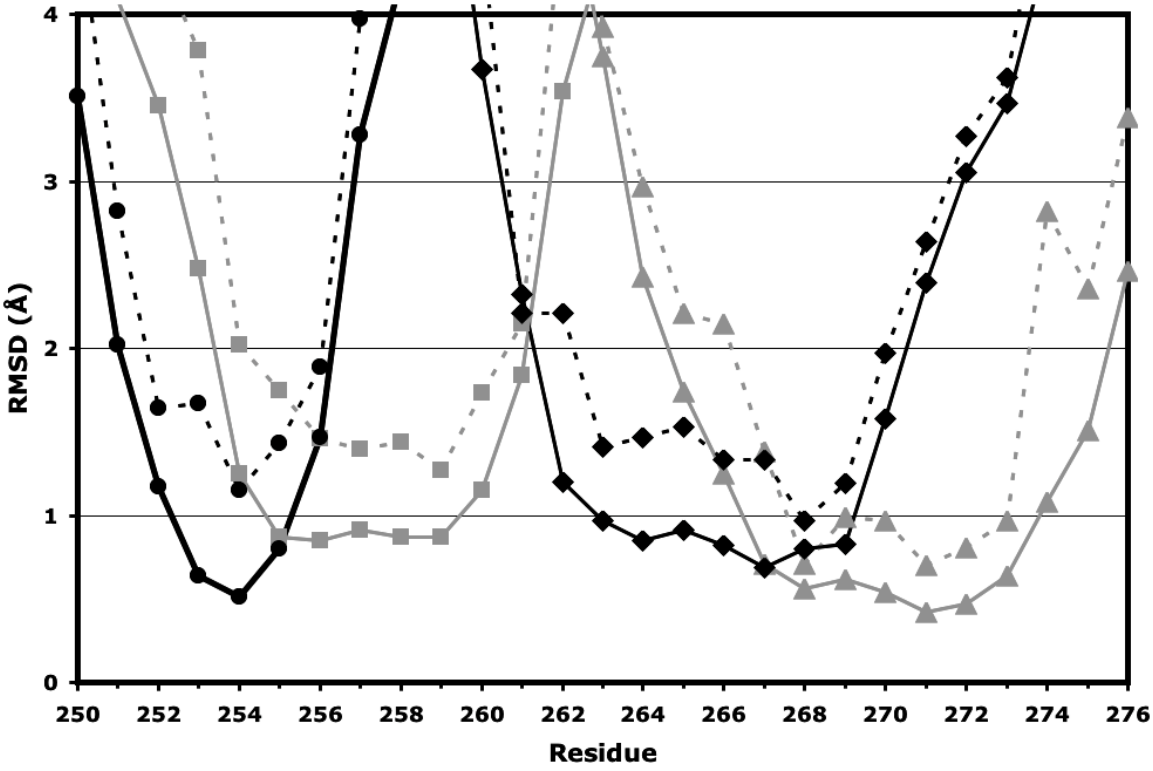

Fig. S1. – RMSD over structurally convergent segments of TM VII peptide in DPC micelles. Solid lines – backbone heavy-atom RMSD; dashed lines – all heavy-atom RMSD. Black circles: segment i – superposed over N252-H256; grey squares: segment ii – superposed over L255-G262; black diamonds: segment iii – superposed over E262 – T270; grey triangles: segment iv – superposed over D267-L273.

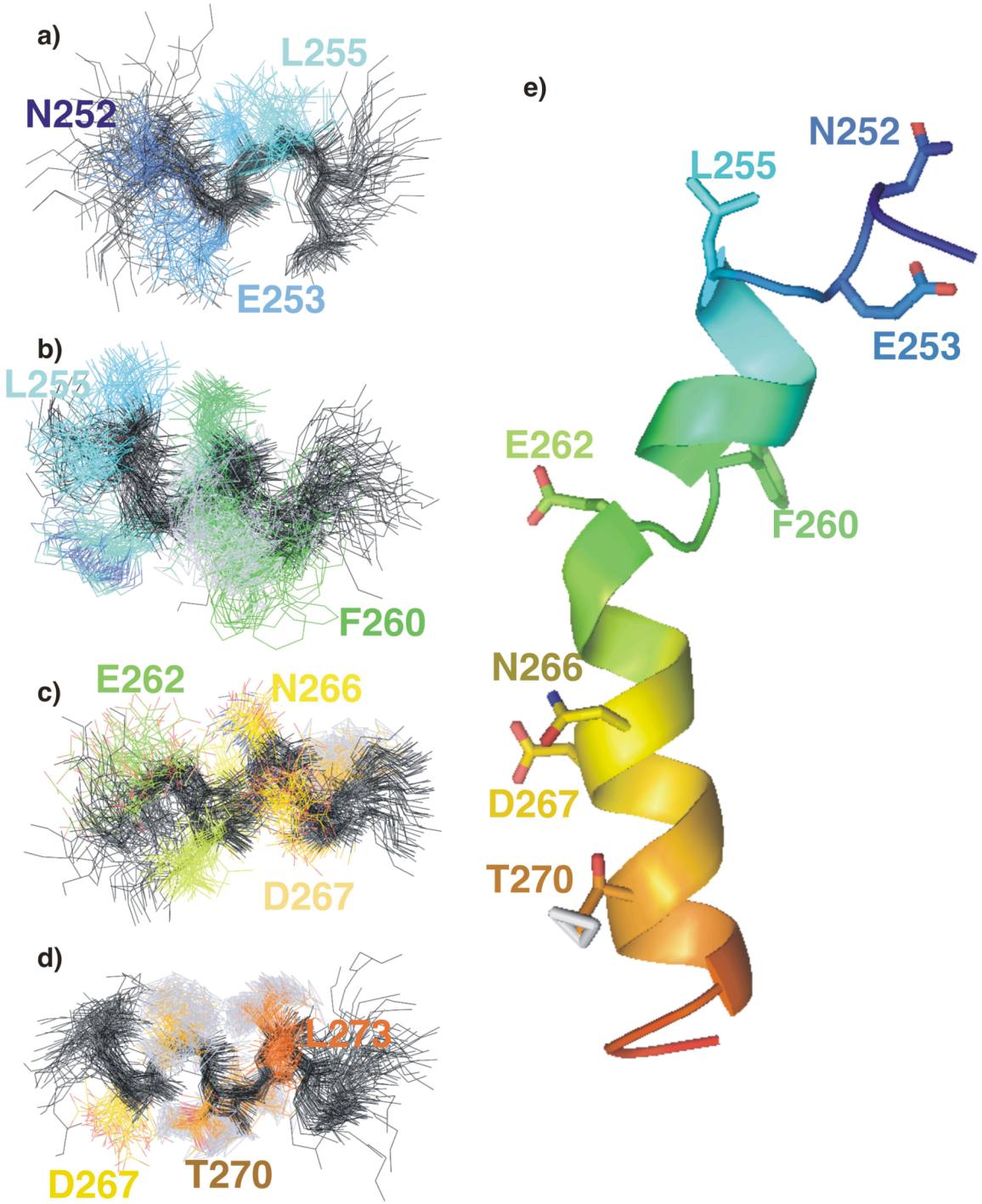

Fig. S2 – Superpositions of ensemble of TM VII structures alongside representative structure. (a)-(d) Superpositions of all ensemble members for segments i-iv shown from Fig. 1. Backbone shown in black in each case, side-chains coloured from blue to red from N- to C-terminal for: (a) H250-I257 backbone; I252-L255 side-chains (b) E252-E262 backbone; L255-F260 side-chains (c) F260-T270 backbone; E262-V269 side-chains, and (d) L264-K276 backbone; D267-L273 side-chains. (e) Representative structure shown in Fig. 9 of accompanying paper provided as frame of reference (colouring same as in (a)-(d)). Note: methyl groups on side-chains appear as grey triangles.